How to cite: *Angew. Chem. Int. Ed.* **2022,** *61,* e202116041
International Edition: doi.org/10.1002/anie.202116041
German Edition: doi.org/10.1002/ange.202116041

Nanomotors

Generic Rules for Distinguishing Autophoretic Colloidal Motors

*Yixin Peng, Pengzhao Xu, Shifang Duan, Jiayu Liu, Jeffrey Lawrence Moran, and Wei Wang**

Abstract: *Distinguishing the operating mechanisms of nano- and micromotors powered by chemical gradients, i.e. "autophoresis", holds the key for fundamental and applied reasons. In this article, we propose and experimentally confirm that the speeds of a self-diffusiophoretic colloidal motor scale inversely to its population density but not for self-electrophoretic motors, because the former is an ion source and thus increases the solution ionic strength over time while the latter does not. They also form clusters in visually distinguishable and quantifiable ways. This pair of rules is simple, powerful, and insensitive to the specific material composition, shape or size of a colloidal motor, and does not require any measurement beyond typical microscopy. These rules are not only useful in clarifying the operating mechanisms of typical autophoretic micromotors, but also in predicting the dynamics of unconventional ones that are yet to be experimentally realized, even those involving enzymes.*

Introduction

Colloidal motors are artificial objects that convert energy stored in their environment into autonomous motion.[1] They are useful model systems for studying active matter and non-equilibrium phenomena[2] and could enable functional micro- and nanorobots in a wide range of applications.[3] Developing effective propulsion mechanisms, and understanding how they operate, remains a key issue in both fronts.

Many colloidal motors are powered by surface chemical reactions.[4] Some move by converting ambient chemical fuels into neutral molecules that either nucleate into bubbles[5] or create an osmotic flows.[6] These two mechanisms are relatively easy to identify, because in neither case does the speed change upon adding salt, and the former often leaves a trace of bubbles. On the other hand, many phoretic motors produce and/or consume ions, which then generate an electric field that propels a charged colloidal motor.[7] Such an electrokinetic process can occur via either self-electrophoresis,[8] where ions are produced and consumed at different parts on a motor. It can also occur via ionic self-diffusiophoresis,[9] where a motor produces both cations and anions and consumes neither. Knowing which mechanism is in operation not only explains the individual propulsion of a colloidal motor, but more importantly, clarifies their communication,[10] self-assembly,[2c,11] collective behaviors[12] and dynamics in a complex environment.[13] Note that, for simplicity, the term "self-diffusiophoresis" is used throughout this article to refer only to the ionic (electrolyte) type. Neutral self-diffusiophoresis is not considered in detail in this paper, because experimental evidence is rare,[6a] and its presence can be easily identified by adding salt. Much of the ambiguity, however, lies between ionic self-diffusiophoresis and self-electrophoresis.

Although self-diffusiophoresis and self-electrophoresis entail different distributions of ions, electric fields, and flows, distinguishing them during the operation of a colloidal motor remains a challenge: in both mechanisms, a colloidal motor slows down as ionic strength is increased.[14] They also attract or repel charged tracer particles and/or obstacles in virtually indistinguishable ways. Resolving this problem often involves two steps. First, the exact chemical reaction and species involved need to be identified, but this is often challenging particularly when intermediates are considered,[14a,b] or if more than one chemical reaction (or multiple pathways of the same reaction) occur.[14b,15] Second, local chemical[16] or flow profiles[17] need to be measured precisely (e.g., with fluorescent probes and/or tracer nanoparticles), but the steep learning curves and possible interferences and caveats of these fine measurements limit their widespread use. Simply put, the real yet subtle differences between self-electrophoresis and self-diffusiophoresis are impossible to visualize using straightforward microscopy, a problem that has haunted experimentalists like us for a long time. At a fundamental level, this problem has greatly obscured the picture of how chemical motors operate individually or collectively, and has thus contributed to the divide between theoretical predictions and experimental observations of colloidal motors. This challenge also hampers societal adoption of colloidal motors since a lack of knowledge of their inner workings prevents us from knowing exactly what tasks they may (or may not) be useful for.

To address this issue, we here report a pair of empirical rules for experimentally distinguishing self-electrophoresis and self-diffusiophoresis during their operation by examining their speeds at different population densities, and how they cluster. These rules build upon the fundamental differ-

[*] Y. Peng, P. Xu, S. Duan, J. Liu, Prof. W. Wang
Sauvage Laboratory for Smart Materials, School of Materials Science and Engineering
Harbin Institute of Technology (Shenzhen)
Shenzhen, Guangdong, 518055, China
E-mail: weiwangsz@hit.edu.cn
Prof. J. L. Moran
Department of Mechanical Engineering
George Mason University
Manassas, VA 20110 (USA)

ence that (in the most typical cases) a self-diffusiophoretic motor is an ion source that continuously increases the local (and the bulk) ionic strength (confirmed in Figure 3), whereas a self-electrophoretic motor does not (see Figure 1 for an illustration of this principle). The core impact of a raised ionic strength is a reduction of self-propulsion speeds, commonly attributed to an increase in surface conductance that reduces the magnitude of the self-generated electric fields.[14a,c,18] Two rules then follow. Rule #1: a self-diffusiophoretic motor moves more slowly in a denser population due to the overlapping ion clouds of neighboring motors, while self-electrophoretic motors maintain an almost constant speed regardless of population density (Figure 4). Rule #2: self-diffusiophoretic motors form clusters that grow over time with an increasing rate, while self-electrophoretic motors form dynamic clusters with limited sizes (Figure 5). Six types of well-studied phoretic colloidal motors of both spherical and rod shapes are used to validate these rules. Our proposed rules suggest that PS-Pt and SiO_2-TiO_2 Janus motors are self-electrophoretic rather than self-diffusiophoretic (Figure 6). Moreover, our rules can also predict the speeds and clustering of four types of atypical phoretic motors at high population densities. This article ends with a comment on the far-reaching consequences of our study in clarifying the fundamental operations of chemical micro- and nanomotors.

Results and Discussion

Principles of the Empirical Rules

We begin with a brief introduction to the operating principles of self-electrophoresis and self-diffusiophoresis, which lead to the principles of the rules.

For a typical self-electrophoretic motor (Figure 1a–d), part of its surface contains a chemically active material that releases ions, which are consumed at other parts of the particle surface in such a way that the total ionic current into or out of the particle surface is zero at steady state. These processes often occur on the separate ends of a colloidal motor (such as two opposing caps of a Janus microsphere,[19] two ends of a conductive carbon fiber,[20] or two segments of a microrod[21]). The resulting distribution of ions creates an electric field that points from regions of an excess of cations to regions of their depletion.[22] When coupled to a colloidal particle carrying a surface charge (often negative), this self-generated electric field moves the particle by electrophoresis, thus the name self-electrophoresis.[8,15b] Typical examples include bimetallic microrods (or spheres) moving in H_2O_2 (such as the Au-Pt spheres and Au-Rh rods we use below),[19a,23] and Janus microspheres containing a semiconductor-metal junction (such as the TiO_2-Pt spheres we use below).[24] Importantly, because self-electrophoretic motors generate and consume the same ions simultaneously (an ion "source" and "sink", Figure 1b), at steady state a self-electrophoretic motor produces no net ions over time regardless of the population density.

On the other hand, a self-diffusiophoretic motor (Figure 1e–h) often contains a single chemically active cap or

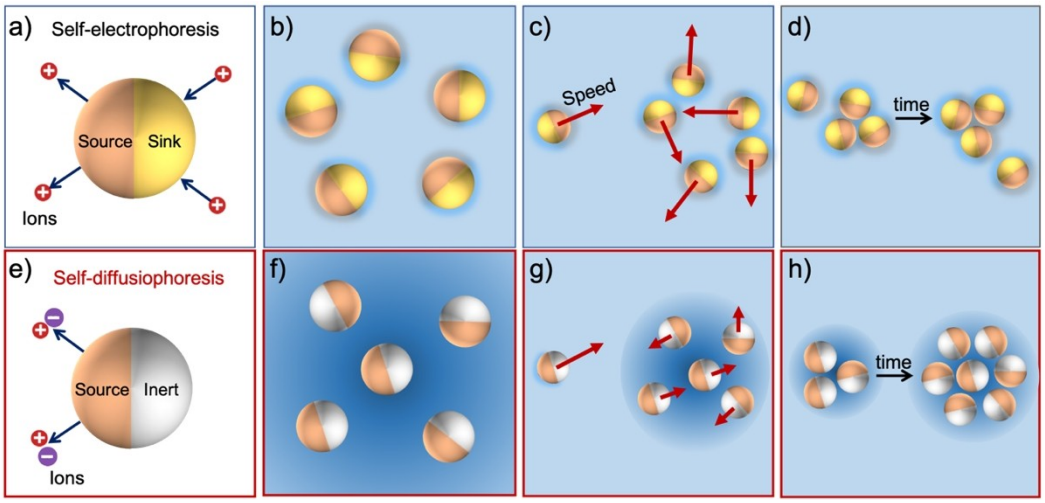

Figure 1. Principles for differentiating self-electrophoretic (a)–(d) from self-diffusiophoretic (e)–(h) colloidal motors. a) A self-electrophoretic motor releases ions on one side ("source") and consumes them on the other ("sink"). As a result, self-electrophoretic motors do not increase the bulk ionic strength (b), maintain largely the same speed when moving in a dense population (c), and form dynamic clusters that reach a steady, but limited, size over time (d). e) A self-diffusiophoretic motor releases ions (typically both positive and negative ions simultaneously) on part of its surface ("source"), while the rest of the particle is inert. As a result, they continuously raise both the local and bulk ionic strength (f), exhibit slower speeds in a dense population (g), and form clusters that grow over time (h). In panels (b)–(d) and (f)–(h), darker and lighter shades of blue indicate higher and lower local ionic strength, respectively.

patch, which typically releases ions. Unlike the case of self-electrophoresis, these ions are not consumed elsewhere on the particle surface. In addition, cations and anions are often released together to conserve charge. In the typical case that these two ions diffuse at different rates, an electric field is generated to maintain charge neutrality in the bulk solution by accelerating the slower ion and slowing down the faster one.[25] This electric field then propels a charged colloidal motor.[26] Note that the origin of this self-generated electric field is a difference of diffusivity in the released cation and anion, rather than the space charges as in the case of self-electrophoresis. Examples of self-diffusiophoretic motors include insert colloids partially coated with silver chloride (AgCl), which reacts with water to produce Cl^- and H^+ under light,[26b,27] or coated with calcium carbonate ($CaCO_3$) that dissolves in water to release Ca^{2+}, OH^-, CO_3^{2-} and HCO_3^-.[28] Some enzyme-powered colloidal motors also fall into this category.[29] The most important feature of a self-diffusiophoretic motor in the current context is that it effectively acts as an ion "source" (Figure 1e) that raises the local and bulk ionic strength over time.

The above principles regarding ionic strength lead to a testable experimental prediction: since both types of motors move more slowly in response to increased ionic strength (see our descriptions above, and Refs. [14a,b,18]), and since self-diffusiophoretic motors raise the local ionic strength while self-electrophoretic ones do not change it, observable differences will arise in the speeds and clustering dynamics of the motors as their population density increases (Figure 1). At a single-particle level, if the population density of self-diffusiophoretic motors is high, each individual motor is affected by the overlapping electrolyte concentration fields from its neighbors, increasing the local ionic strength surrounding each motor, reducing its speed as if it were immersed in a concentrated salt solution. However, a self-electrophoretic motor will maintain virtually the same speed even when in proximity to other motors because there is no net electrolyte production (see below for why this is not strictly true). This is rule No.1. At a cluster level, the overlapped electrolyte concentration field of a self-diffusiophoretic cluster pulls nearby motors in; since each motor moves too slowly to escape, the cluster continuously grows. In contrast, self-electrophoretic motors form a dynamic cluster with a limited size because each motor still moves at the same speed as it would on its own (outside a cluster) and can escape. This is rule No.2. Self-electrophoretic and self-diffusiophoretic motors can thus be distinguished by examining their speeds at increasing population densities, and by observing how they form clusters.

Experimental Validation of Rules

We experimentally validated this pair of rules using six types of colloidal motors of known composition: three self-electrophoretic (Au-Pt and TiO_2-Pt microspheres, and Au-Rh bimetallic microrods) and three self-diffusiophoretic designs (SiO_2-Au and SiO_2-Ag microspheres, and SiO_2-Ag microrods). The propulsion mechanisms and typical dynamics of these motors are shown in Figure 2, while the details on their fabrication and material characterization (Figure S11) are given in the Supporting Information. Note that the typical speeds of all motors in their dilute limits are on the same order of magnitude of approximately 10 $\mu m\,s^{-1}$.

Au-Pt and TiO_2-Pt Janus microspheres as well as Au-Rh bimetallic microrods are typical designs of self-electrophoretic motors (Figure 2a–c). A Au-Pt self-electrophoretic microsphere (Figure 2b) can be fabricated by half-coating a Au or Au-coated microsphere with Pt via physical vapor deposition (PVD).[19a,30] A Au-Rh rod (Figure 2c), on the other hand, is typically grown by template-assisted electrodeposition.[21b] When such a bimetallic motor is suspended in an aqueous solution of H_2O_2, H_2O_2 is oxidized into O_2 and protons at the anode (Pt or Rh) end, whereas H_2O_2 (and, to some extent, O_2) combine with protons to be reduced into water at the cathode (Au) end. As a byproduct of these bipolar electrochemical reactions, a self-generated electric field is created (pointing from the Pt/Rh to the Au

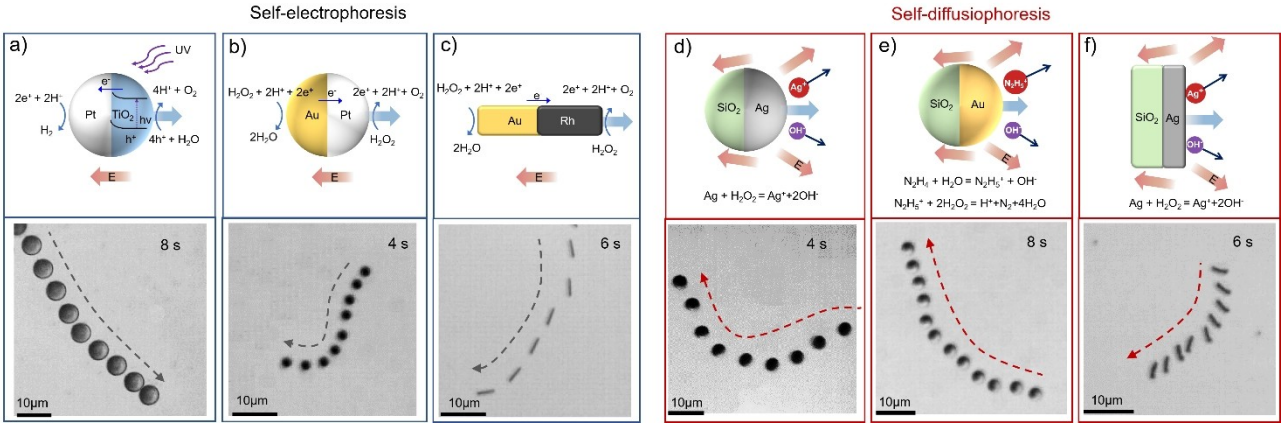

Figure 2. Model systems of autophoretic colloids for testing rules. Top: Schematics of the propulsion mechanisms of three self-electrophoretic motors (a: TiO_2-Pt, b: Au-Pt, c: Au-Rh rods) and three self-diffusiophoretic motors (d: SiO_2-Au, e: SiO_2-Ag, f: SiO_2-Ag rods). Bottom: Representative trajectories of each type of motors overlaid over a few seconds. See Supporting Information for experiment details.

end) that propels the negatively charged motor with the Pt/Rh end forward. A similar process also occurs on a TiO_2-Pt Janus microsphere (Figure 2a), which is fabricated by depositing Pt on one side of a TiO_2 microsphere that is chemically synthesized. In the presence of a fuel molecule (such as water,[24d] hydrogen peroxide,[24c] hydroquinone[24a] or triethylamine[31]) and light of proper wavelength, photocatalysis generates an excess of protons on the TiO_2 side, which are transported to the Pt side and consumed in the reduction of H_2O_2. This motor then moves with its TiO_2 end forward via self-electrophoresis. Crucially, none of the three types of self-electrophoretic motors cause any net production or consumption of ions at steady state since the total reaction rates on the anode and cathode are equal.

As representative self-diffusiophoretic motors, SiO_2-Au and SiO_2-Ag micromotors (Figure 2d–f) were fabricated by PVD of the respective metal onto one half of a SiO_2 microsphere (or the side of a SiO_2 rod in the case of a SiO_2-Ag microrod). A recent study by the Gao group[32] shows that SiO_2-Ag Janus microspheres (Figure 2c) self-propel toward their Ag caps in aqueous solutions of H_2O_2, likely because of the oxidation of Ag by H_2O_2 into Ag^+ and OH^-, which diffuse at different rates and thus move the colloid via self-diffusiophoresis. A SiO_2-Ag microrod also moves in H_2O_2 via the same mechanism.[32b] A SiO_2-Au Janus microsphere (Figure 2d), on the other hand, moves in a mixture of N_2H_4 and H_2O_2,[33] as the Au cap catalyzes the oxidation of N_2H_4 and generates H^+, $N_2H_5^+$ and OH^- that diffuse at different rates away from the Au cap, leading to propulsion by self-diffusiophoresis. It is then reasonable to speculate that ions are produced only on the metal caps of both SiO_2-Au and SiO_2-Ag Janus micromotors, making them ion sources.

For simplicity, only the results of spherical micromotors are given below, while those of rod-shaped motors are qualitatively the same as their spherical counterparts and therefore shown in Figure S8 in the Supporting Information.

Figure 3 aggregates the experimental and numerical evidence suggesting that self-diffusiophoretic motors are ion sources and self-electrophoretic motors produce no net ions. Specifically, Figure 3a and b show experimental measurements of much more significant increases in the electrical conductivity (σ) of aqueous suspensions of self-diffusiophoretic motors (SiO_2-Ag and SiO_2-Au) than self-electrophoretic motors (Au-Pt and TiO_2-Pt) of similar speeds during their operation. (The population density φ is determined by

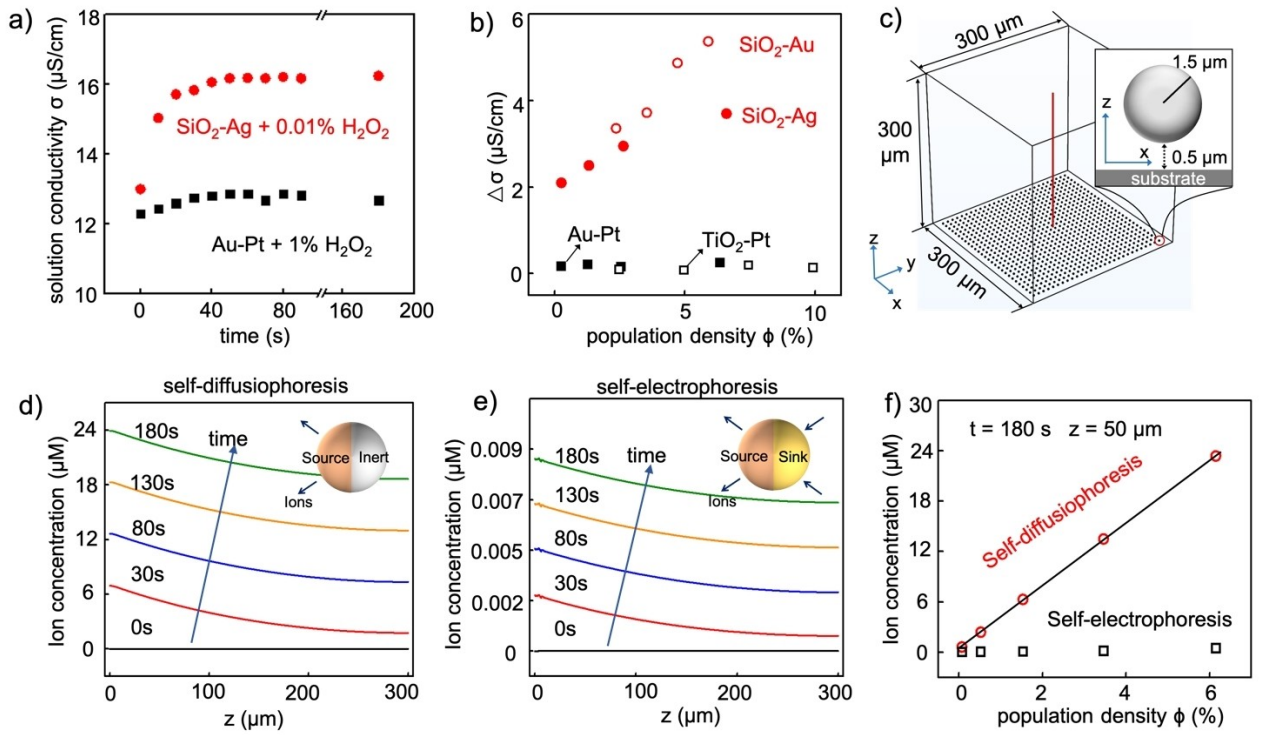

Figure 3. Changes in global ionic strength by autophoretic colloids. a) Experimentally measured electrical conductivity (σ) of suspensions of SiO_2-Ag microspheres (in 0.01 %wt H_2O_2) and Au-Pt (in 1 wt% H_2O_2) over time. b) Increases in solution conductivity ($\Delta\sigma$) of aqueous solutions of SiO_2-Au (5 wt% H_2O_2 and 0.01 wt% N_2H_4), TiO_2-Pt (in water, under UV), SiO_2-Ag, and Au-Pt motors at different population densities. These results were obtained after the conductivity values reached steady state (80 s). c–f) Numerical simulations of the changes in solute concentrations in suspensions of autophoretic colloids. c) Model configuration, containing an array of 28×28 (=784) microspheres at a population density of 6.3 %. Particles settle close to a substrate because they are typically heavier than water. d, e) Solute concentration profiles along the red cutline in (c), as a function of time, for self-diffusiophoretic motors (d) and self-electrophoretic motors (e). Note the y axes in (d) and (e) are in different scales. f) Simulated solute concentration at $z = 50$ μm along the red cutline in (c) and at $t = 180$ s for both types of motors at different population densities.

the packing fraction of colloids on a 2D plane they reside on, enabled by computer-assisted image recognition. See Figure S1 for details.) To corroborate these results, numerical simulations were performed that solved for the spatiotemporal evolution of solute concentrations in a closed box containing either type of motor of various population densities. Results shown in Figure 3c–f agree qualitatively with the measurement of solution conductivity: the solute concentration in the bulk increases linearly with the population density of a suspension of self-diffusiophoretic motors, but remains unchanged for self-electrophoretic motors. More quantitatively, our models yield a solution conductivity of 6.1 $\mu S\,cm^{-1}$ for SiO_2-Ag motors of 6.3 % population density (See Supporting Information for calculations), close to the experimentally measured value of 3.5 $\mu S\,cm^{-1}$ shown in Figure 3b. The above results confirm the significant rise of solution conductivity by the ions released from self-diffusiophoretic motors but not self-electrophoretic motors.

Rule #1: Motor Speeds vs. Population Density

To confirm that the speed of self-diffusiophoretic motors decreases with increasing population density much more than the speed of self-electrophoretic motors, we measured the speeds at a variety of population densities for all six types of phoretic motors in their respective operating conditions (Note that SiO_2-Au motors were tested at an oil-water interface, with justification and experimental details given in the Supporting Information). Results of the spherical and rod-shaped motors are shown in Figure 4 and Figure S8a, respectively (also see Supporting Video S1). Figure 4a clearly shows that the speeds of self-diffusiophoretic SiO_2-Au and SiO_2-Ag motors drop sharply upon increasing their population densities, much more so than self-electrophoretic TiO_2-Pt and Au-Pt motors. The latter two also slow down (but quite mildly) in a crowd instead of maintaining a constant speed as expected from the conductivity argument, likely because of the same steric hindrance ("traffic jams") that caused the "motility induced phase separation", or MIPS.[34]

More quantitatively, Figure 4b further shows that the speeds of self-diffusiophoretic motors scale *inversely* with their population densities, but the same is not true for self-electrophoretic motors. Furthermore, a similar scaling between motor speeds and ionic strength was found in Figure 4c regardless of whether the solution ionic strength was adjusted manually (by adding KNO_3, see Figure S5 for raw data) or by the motors themselves, suggesting that diffusiophoretic motors indeed slow down in their own generated ions. Possible reasons for the deviation of speed data from a linear fit in Figure 4b and c in their dilute limits are discussed in the Supporting Information (see Figure S12 and Figure S13).

Rule #2: Self-Diffusiophoretic and Self-Electrophoretic Motors Cluster Differently

Clustering is ubiquitous in populations of colloidal motors,[11a,c,34a,35] especially for those powered by chemical gradients.[16b,23a,b,24d,36] The second rule is that self-diffusiophoretic motors tend to form "static" clusters that grow over time, while self-electrophoretic motors form "dynamic" clusters of a relatively steady size (see Figure 5, Supporting Video S2). This rule again is rooted in their differences in ion production and consumption, as elaborated below.

To validate this rule, Figure 5a shows the clustering of self-diffusiophoretic SiO_2-Ag motors (top panel, $\varphi = 13.2\,\%$)

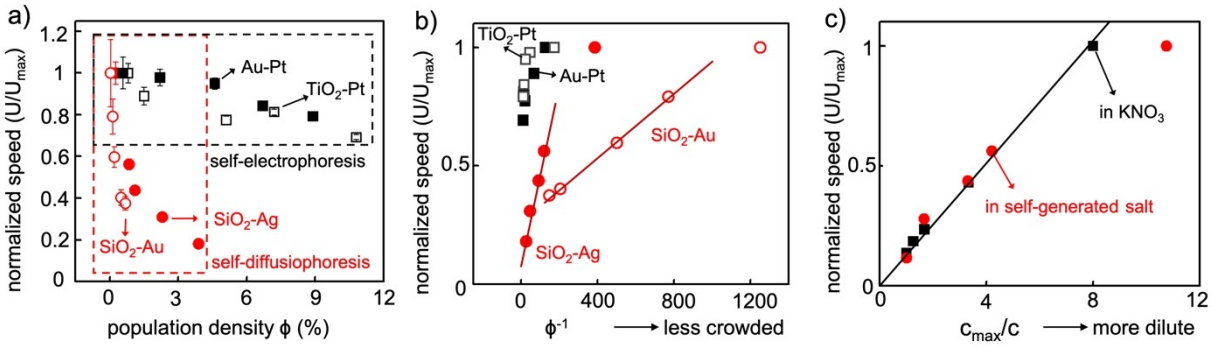

Figure 4. Speeds of self-electrophoretic and self-diffusiophoretic motors in different sized populations. a) Speeds of two types of self-electrophoretic motors (TiO_2-Pt, hollow squares and Au-Pt, filled squares) and two types of self-diffusiophoretic motors (SiO_2-Au, hollow circles and SiO_2-Ag, filled circles) at different population densities. Data of higher population densities for SiO_2-Au were not possible because of they easily form clusters that disable single particle tracking. Error bars represent standard errors from each independent measurement, and the samples (number of particles) increases as the population density. b) Data in a) replotted against inverse population density, φ^{-1}. Solid lines are linear fits of the first four data points. c) Speeds of SiO_2-Ag motors scale roughly to the inverse of salt concentrations. Both the speeds and the solute concentrations are normalized to their maxima. Data in black squares correspond to the speeds SiO_2-Ag motors in manually added KNO_3 (original data in Figure S5). Data in red circles are for self-generated salts, inferred by combining the simulated results in Figure 3f (relating c with φ) and the experimental results in Figure 4a (relating φ with U). The solid line is a linear fit of the black data points through the origin. Possible reasons for the deviation of the red curve from the linear fits are given in the main text.

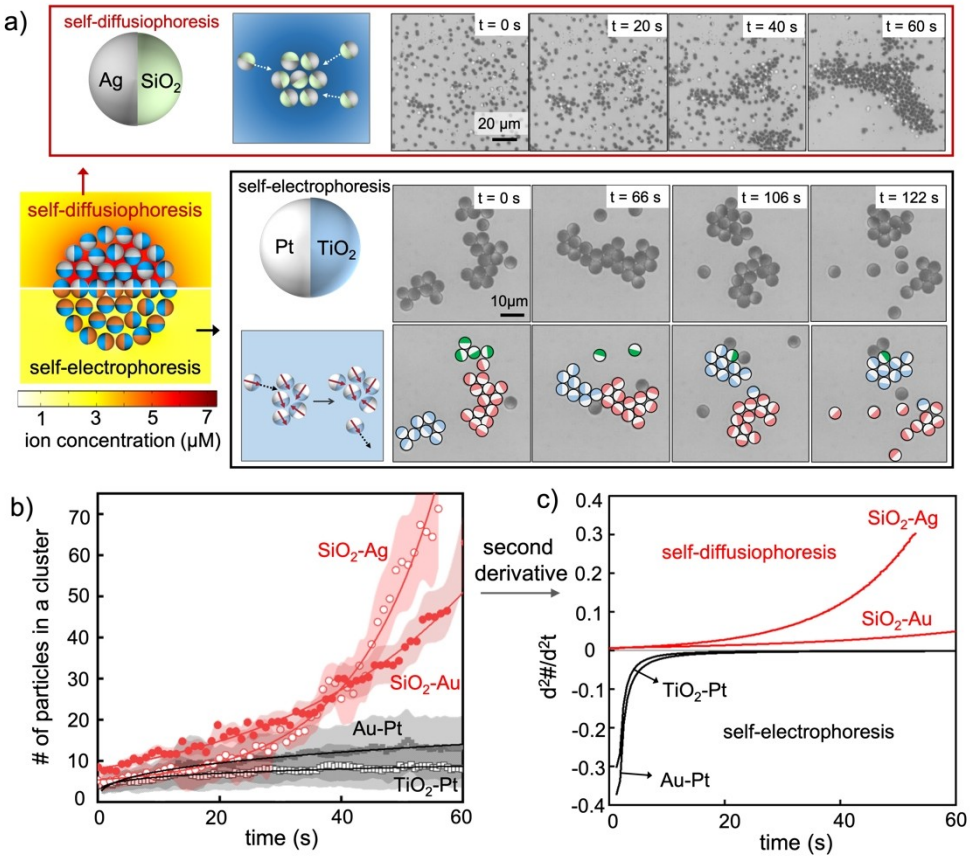

Figure 5. Clustering dynamics of self-electrophoretic and self-diffusiophoretic motors. a) Cartoon illustrations and optical micrographs of the clustering processes of self-diffusiophoretic SiO_2-Ag motors (top) and self-electrophoretic TiO_2-Pt motors (bottom). The micrographs for TiO_2-Pt motors are overlaid with cartoons that show the evolution of three clusters (labelled red, blue and green) over a course of 122 s. Inset in a) shows the simulated ion concentrations of a self-diffusiophoretic (top half) and a self-electrophoretic cluster (bottom half) at $t = 10$ s stitched together. The orientations of Janus spheres are random in either cluster. See Supporting Information for simulation details. b) The evolution of cluster sizes (represented by the average number of particles in each cluster) for self-diffusiophoretic SiO_2-Ag and SiO_2-Au motors (hollow and filled red circles, respectively), and self-electrophoretic TiO_2-Pt and Au-Pt motors (hollow and filled black squares, respectively). Shades represent standard deviations of all clusters. Solid lines are parabolic fits ($R^2 > 0.97$). c) The parabolic fits in (b) are taken second derivatives with respect to time and plotted against time, yielding positive values for self-diffusiophoretic motors (red) and negative for self-electrophoretic motors (black). First derivatives are given as Figure S6 in Supporting Information. Experiments of SiO_2-Ag, SiO_2-Au, TiO_2-Pt, and Au-Pt motors were carried out at a population density of 13.2%, 10.5%, 12.4% and 11.8%, respectively.

and self-electrophoretic TiO_2-Pt motors (bottom, $\varphi =$ 12.4%) as examples (results of the other four types of motors are given in Figures S8 and S9). In such a dense population, SiO_2-Ag motors lose their self-propulsion because an increase in local ionic strength is known to suppress electrokinetic flows.[14a,c,18] They therefore formed a large cluster that continued to phase separate. In lieu of electrokinetic flows, these diffusiophoretic clusters are speculated to form because of neutral diffusio-osmosis in a gradient of H_2O_2 and O_2 that pulls colloids in regardless of their orientations, whereas other mechanisms such as chemotaxis[37] and MIPS[34b,c] are inoperative. Electrostatic repulsions and van der Waals attractions are not considered because clustering in our experiments is clearly activity-induced and disappear when self-propulsion ceases (see Figure S10). However, the exact physical mechanism of cluster formation of chemically active colloids remains an ongoing investigation and not a focus of the current study.

Self-electrophoretic TiO_2-Pt motors, on the other hand, remained highly mobile and were continuously exchanged among clusters (see optical micrographs and cartoons in Figure 5a, bottom panel), because of a lack of high ionic strength that slows them down in a cluster. As a result, these clusters constantly split and reorganized, and saturated to certain sizes with a cluster growth rate that decreased over time. Similar observations of dynamic clustering have been reported previously.[23b,c,34a]

The change in the cluster sizes over time of four types of colloidal motors is plotted in Figure 5b, all showing positive growth (and positive values of first derivatives against time, see Figure S6). Therefore, to avoid ambiguity, we note that the first and second derivatives of cluster size with respect to time are both positive for the self-diffusiophoretic motor clusters, while only the first derivatives are positive for clusters of self-electrophoretic motors. These operations are

necessary for a definitive rule to distinguish these two types of motors.

Applying the Rules to Other Motor Systems

Having proposed and validated the 2 rules for distinguishing between self-diffusiophoretic motors and self-electrophoretic motors, we now seek to apply these rules to two additional colloidal motors whose propulsion mechanisms remain unsettled. The first test was on the Pt-coated Janus microspheres. In the early days of its discovery, the motion of these motors was attributed to neutral self-diffusiophoresis,[38] which was proposed to arise from a concentration gradient of neutral solutes, such as O_2, that are generated around the Pt cap as it catalyzes the decomposition of H_2O_2. However, recent studies have discovered that Pt-coated micromotors slow down in solutions of high ionic strength,[14a,b,18a] and that Janus spheres half-coated with discrete Pt nanoparticles move much more slowly than ones coated with continuous Pt films despite their similar catalytic activity.[39] Neither observation is consistent with neutral self-diffusiophoresis. A variety of alternative mechanisms have been proposed,[14a,b,15a,38,40] with self-electrophoresis gaining momentum.[17,39] But more experimental support is still required.

Applying our rules to PS-Pt micromotors, however, clearly reveals that they exhibit the key experimental features of a self-electrophoretic motor (see Figure 6, Supporting Video S3 and Supporting Video S4). Specifically, Figure 6a and b show a mild decrease of PS-Pt motor speeds as population density increased that is far from a 1/φ scaling, and Figure 6c and d show that PS-Pt clusters grow slowly with a negative second derivatives over time. Figure 6e further illustrates how PS-Pt clusters are dynamic and motile. All three observations are consistent with features of self-electrophoretic rather than self-diffusiophoretic motors.

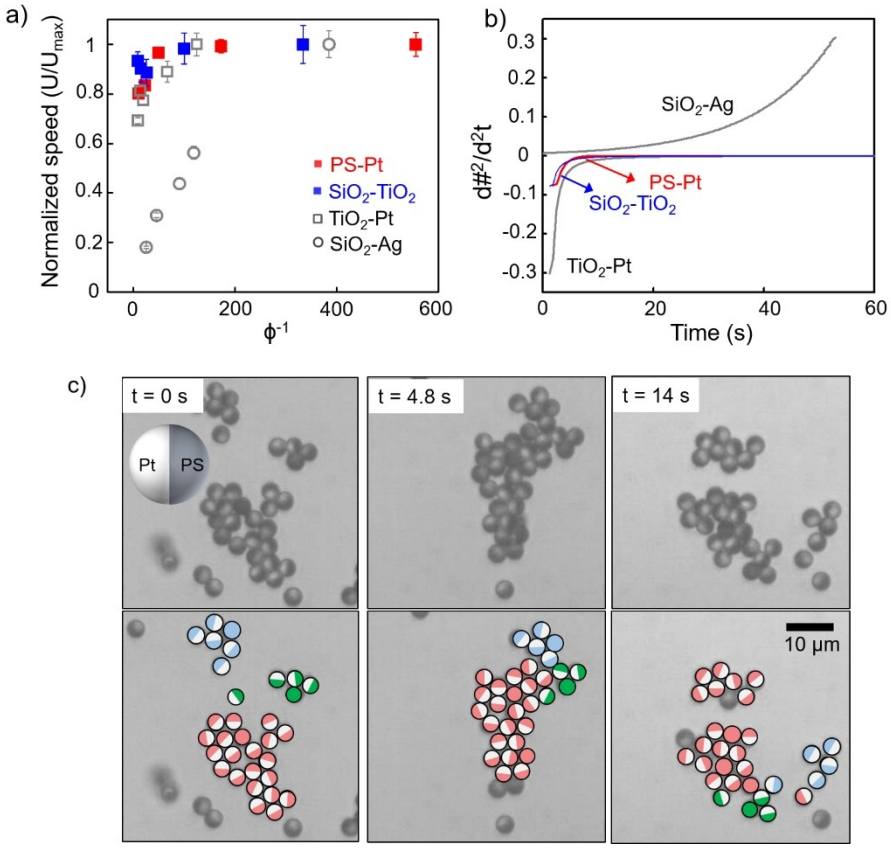

Figure 6. Applying the rules to distinguish the propulsion mechanisms of SiO_2-TiO_2 and PS-Pt motors. a) Normalized speeds of SiO_2-TiO_2 (blue filled squares) and PS-Pt (red filled squares) motors at different population densities. Speeds data of SiO_2-Ag (hollow circles) and TiO_2-Pt motors (hollow squares) from Figure 4a are also plotted here to represent self-diffusiophoretic motors and self-electrophoretic motors, respectively. All speeds are normalized to the speed at their lowest population density (i.e. speed maxima). Error bars represent standard errors from each independent measurement, and the samples (number of particles) increases as the population density. b) Second derivative of the cluster sizes of SiO_2-TiO_2 and PS-Pt over time. The evolution of SiO_2-Ag and TiO_2-Pt clusters are plotted in grey for reference. c) Optical micrographs of the clustering processes of PS-Pt motors. The bottom row is overlaid with colored cartoons to highlight the dynamics of three clusters. Experiments of SiO_2-TiO_2 were carried out in aqueous solutions containing 5 wt% hydroquinone irradiated with UV light of 114 mW cm^{-2}, at a population density of 11.9%. Experiments of PS-Pt were performed in 1 wt% H_2O_2, at a population density of 9.2%. Original data for (a) and (b) are shown in Figure S7.

We have also applied the same rules to SiO_2-TiO_2 Janus micromotors, which are fabricated by evaporating TiO_2 on one side of SiO_2 microspheres. They are known to self-propel away from the TiO_2 caps under UV irradiation via photocatalysis.[41] Although self-diffusiophoresis has been suspected to be its operating mechanism,[9a,41a,42] our results in Figure 6 and Figure S7 clearly show that SiO_2-TiO_2 motors, like PS-Pt, are self-*electrophoretic.* The most popular speculation for a Pt motor to be self-electrophoretic is to consider the uneven thickness of a Pt cap,[14a,b,17] but it is difficult to imagine how the thickness variation of a TiO_2 cap could alter its catalytic performance. However, a study from Brook et al.[15a] has predicted the operation of self-electrophoresis for a both a Pt- and a TiO_2-coated Janus colloidal motor without invoking the thickness argument, and could thus reconcile with our observations. More efforts are clearly needed to clarify the operating mechanism of a SiO_2-TiO_2 motor, a topic that is rarely explored.

Reliability of the Six Model Systems

Uncertainties exist for the six motor systems used to corroborate our rules, related to the details of their chemical reactions and operating mechanisms. For example, a few studies have revealed the possible (yet to a lesser degree) presence of self-diffusiophoresis in the case of bimetallic rods[43] or pumps[44] that are commonly considered to be self-electrophoretic. Nevertheless, it is still generally agreed that self-electrophoresis[8,15b,45] is the dominant mechanism for TiO_2-metal and bimetallic motors used in this article. On the other hand, the mechanisms for SiO_2-Au motors moving in H_2O_2 and N_2H_4 and SiO_2-Ag motors in H_2O_2, although reasonably speculated to be ionic self-diffusiophoresis, have not reached general consensus yet. Besides, the inevitable catalytic decomposition of H_2O_2 on the surface of Au or Ag could cause complications, yet this was not considered in our models.

Despite these caveats, the speed data and clustering dynamics of all six systems consistently show agreement between the three within the same category and resonate with the reasonable arguments based on ion sources/sinks, lending credibility to the proposed rules.

Applicability of Our Rules to Atypical Autophoretic Motors

Throughout this article, we have defined self-electrophoretic motors as those being both an ionic source and a sink, and self-diffusiophoretic micromotors being only ionic sources. These are the most typical cases in the literature, yet it is theoretically possible to envision other possibilities. Below, we describe how our rules can qualitatively predict the dynamics of four atypical kinds of phoretic micromotors at large populations and during clustering.

The first kind is a Janus micromotor that, on one side of its body, consumes and releases two types of ions of the same sign (Figure 7a–d). A possible example is an ion exchange resin particle that takes in a metal ion and releases protons on the same side of its Janus body, and thus moves via self-diffusiophoresis. However, unlike a typical self-diffusiophoretic motor, such an ion exchange resin motor produces zero net flux of ions. Therefore, it behaves like a self-electrophoretic motor in that its speed does not drop sharply upon increasing the population density, nor does its cluster grows continuously. This scenario has not been tested, even though ion exchange resin microspheres have been used in studies of active colloids.[16b,46]

A second kind of motor is a twist to a typical self-diffusiophoresis motor, so that ions are *consumed* on one side of its Janus body instead of being released (Figure 7e–h). This motor is therefore an ion *sink* and *reduces* the local and global ionic strength as it moves. Following our arguments throughout this article, this unusual motor would *accelerate* in a dense population without forming clusters, completely opposite to a typical self-diffusiophoretic motor. A possible example is a microparticle infused with an organic base (such as amines). When suspended in dilute HCl, H^+ are constantly neutralized by the microparticle, *reducing* the solution ionic strength.

The third kind is a Janus micromotor that produces one pair of cation and anion on one side, and a different pair on the other (Figure 7i–l). This motor is essentially composed of two diffusiophoretic caps and moves in a direction dictated by the pair of ions with the greater difference in diffusivity. Interestingly, in the case that the self-generated electric field points from one cap to the other, the electric field and flow streamlines (Figure 7j,k) are very similar to those surrounding a typical self-electrophoretic motor. An example of such scenario is a $CaCO_3$ microsphere half-coated with AgCl. The AgCl cap releases H^+ and Cl^-, while the exposed $CaCO_3$ hemisphere releases Ca^{2+}, HCO^{3-} and OH^-. An electric field then points from the $CaCO_3$ to the AgCl cap similar to self-electrophoresis, but the produced ions raise the solution ionic strength. This motor thus follows our rules of self-diffusiophoretic motors for its speeds and clustering. Note that a similar design principle has been recently implemented in a communicating swarm consisting of ZnO rods and ion-exchange microspheres.[16b]

The final kind (Figure 7m–p) is a variation of the third kind, so that one pair of ions is *consumed* on one side of the Janus motor, and a second pair is *produced* on the other side. This motor operates via diffusiophoresis (the same as the above case) yet produces zero net ion flux (opposite to the above case). It therefore behaves like a self-electrophoretic motor and follows the corresponding rules. We are, however, unable to devise a motor that behaves this way.

The unusual configurations and behaviors of the above four types of hypothetical motors blur the boundaries between self-diffusiophoresis and self-electrophoresis, and challenge us to rethink how these two mechanisms are related to each other. This is an interesting topic that deserves further consideration.

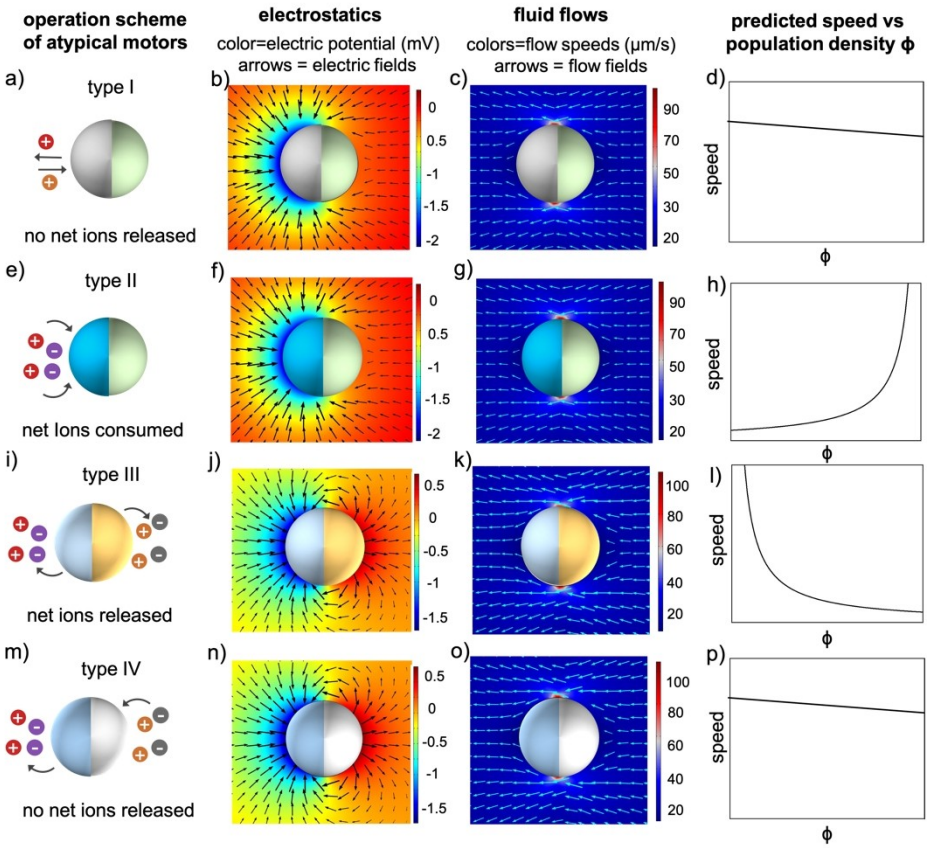

Figure 7. Four types of atypical autophoretic motors (in the same order of their appearance in the main text). Panels a, e, i, and m are schematics of their possible operation. Panels b, f, j, and n are simulated distributions of electrical potential (in colors) and electric fields (in arrows), while panels c, g, k, and o are simulated flow speeds (in colors) and flow fields (in arrows). Panels d, h, l, and p qualitatively illustrate the expected dependence of each motor's speed on population density. The simulations for the bottom two types are for the special cases that produce electric fields pointing from one cap to the other.

Broader Impacts of the Rules

Our proposed rules have far-reaching consequences in clarifying the fundamental operations of chemical micro- and nanomotors. For example, the standard methodology for elucidating a chemical motor typically start from unveiling the nature of the chemical reactions and the identities of the chemical species, followed by an estimate of the gradients, the driving forces, and ultimately the propulsion mechanism. Our rules bypass these steps to work this problem in reverse, by identifying the propulsion mechanism first, which then hints at the chemical details. Moreover, our rules are also critical for understanding and designing chemical motors that communicate with each other and form higher order assemblies,[10a] since each mechanism would predict completely different distributions of chemicals, electric fields and flows, and lead to qualitatively different behaviors (such as the different clustering described above).

Our rules can also help gain fundamental insight into the physics of enzymatic micro- and nanomotors.[47] For example, two enzymes decorated on two ends of a conductive colloid serve as the cathode and the anode, thus propelling the motor via self-electrophoresis.[20,48] Later designs, however, typically functionalize a colloidal particle asymmetrically with enzymes that convert a substrate into molecular or ionic species.[49] They are assumed to be self-diffusiophoretic, but the mechanism is less well defined. Applying our proposed rules (and testing in salts) should clarify the uncertainty.

Conclusion

To conclude, we have presented two empirical rules for experimentally distinguishing ionic self-diffusiophoretic and self-electrophoretic motors that are both driven by electrokinetic flows: 1) the speed of a self-diffusiophoretic motor *scales inversely* with its population density, while self-electrophoretic motors maintain an almost constant speed regardless of their population density (a mild speed decrease is possible in reality), and 2) self-diffusiophoretic motors form clusters with a growth rate that increases over time, while self-electrophoretic motors form dynamic clusters with limited sizes. Both rules originate from the fact that self-diffusiophoretic motors are ion sources that continuously

increase the local and global ionic strength, thus slowing motors down. On the contrary, self-electrophoretic motors are both a source and a sink for ions, producing no net ions. Applying these rules to SiO_2-TiO_2 and PS-Pt motors reveal that they are powered by self-electrophoresis. The dynamics of four types of unconventional phoretic motors can also be predicted with our principles, even though they do not necessarily adhere to a diffusiophoresis or electrophoresis labeling.

This pair of rules is simple, powerful, and insensitive to the specific material composition (metal, polymer or oxides), shape (spheres or rods) or size (micrometer or nanomotor) of a colloidal motor and does not require any measurement beyond typical microscopy. They can be generically applied to phoretic micromotors to understand their mechanisms, including those powered by enzymes.

Acknowledgements

This project is financially supported by the National Natural Science Foundation of China (11774075) and the Shenzhen Science and Technology Program (JCYJ20190806144807401, JCYJ20210324121408022). J.L.M. acknowledges support from start-up funds from the Department of Mechanical Engineering at George Mason University. We are grateful for the helpful discussions with Profs. Mingcheng Yang, Zexin Zhang and Hepeng Zhang, and MATLAB codes from Prof. Hepeng Zhang.

Conflict of Interest

The authors declare no conflict of interest.

Data Availability Statement

The data that support the findings of this study are available from the corresponding author upon reasonable request.

Keywords: Ionic Strength · Micro/nanomotor · Mechanism · Self-Diffusiophoresis · Self-Electrophoresis

[1] a) X. Chen, C. Zhou, W. Wang, *Chem. Asian J.* **2019**, *14*, 2388–2405; b) T. E. Mallouk, A. Sen, *Sci. Am.* **2009**, *300*, 72–77; c) J. Wang, *Nanomachines: fundamentals and applications*, Wiley, Hoboken, **2013**.

[2] a) W. Wang, X. Lv, J. L. Moran, S. Duan, C. Zhou, *Soft Matter* **2020**, *16*, 3846–3868; b) J. Zhang, E. Luijten, B. A. Grzybowski, S. Granick, *Chem. Soc. Rev.* **2017**, *46*, 5551–5569; c) A. Zöttl, H. Stark, *J. Phys. Condens. Matter* **2016**, *28*, 253001; d) D. Needleman, Z. Dogic, *Nat. Rev. Mater.* **2017**, *2*, 17048.

[3] a) J. Parmar, D. Vilela, K. Villa, J. Wang, S. Sánchez, *J. Am. Chem. Soc.* **2018**, *140*, 9317–9331; b) B. J. Nelson, I. K. Kaliakatsos, J. J. Abbott, *Annul. Rev. Biomed. Eng.* **2010**, *12*, 55–85; c) S. A. Mallory, C. Valeriani, A. Cacciuto, *Annu. Rev. Phys. Chem.* **2018**, *69*, 59–79; d) B. Wang, K. Kostarelos, B. J. Nelson, L. Zhang, *Adv. Mater.* **2021**, *33*, 2002047.

[4] a) S. Sánchez, L. Soler, J. Katuri, *Angew. Chem. Int. Ed.* **2015**, *54*, 1414–1444; *Angew. Chem.* **2015**, *127*, 1432–1464; b) B. Robertson, M.-J. Huang, J.-X. Chen, R. Kapral, *Acc. Chem. Res.* **2018**, *51*, 2355–2364; c) A. Nourhani, P. E. Lammert, *Phys. Rev. Lett.* **2016**, *116*, 178302; d) Y. Zhang, H. Hess, *Nat. Chem. Rev.* **2021**, *5*, 550–510.

[5] a) J. G. Gibbs, Y.-P. Zhao, *Appl. Phys. Lett.* **2009**, *94*, 163104; b) A. A. Solovev, Y. Mei, E. Bermúdez Ureña, G. Huang, O. G. Schmidt, *Small* **2009**, *5*, 1688–1692; c) W. Gao, A. Uygun, J. Wang, *J. Am. Chem. Soc.* **2012**, *134*, 897–900.

[6] a) R. A. Pavlick, S. Sengupta, T. McFadden, H. Zhang, A. Sen, *Angew. Chem. Int. Ed.* **2011**, *50*, 9374–9377; *Angew. Chem.* **2011**, *123*, 9546–9549; b) J. F. Brady, *J. Fluid Mech.* **2011**, *667*, 216–259; c) U. M. Córdova-Figueroa, J. F. Brady, *Phys. Rev. Lett.* **2008**, *100*, 158303.

[7] a) J. L. Moran, J. D. Posner, *Annu. Rev. Fluid Mech.* **2017**, *49*, 511–540; b) W. Wang, W. Duan, S. Ahmed, T. E. Mallouk, A. Sen, *Nano Today* **2013**, *8*, 531–554.

[8] W. F. Paxton, P. T. Baker, T. R. Kline, Y. Wang, T. E. Mallouk, A. Sen, *J. Am. Chem. Soc.* **2006**, *128*, 14881–14888.

[9] a) Y. Hong, M. Diaz, U. M. Córdova-Figueroa, A. Sen, *Adv. Funct. Mater.* **2010**, *20*, 1568–1576; b) M. E. Ibele, P. E. Lammert, V. H. Crespi, A. Sen, *ACS Nano* **2010**, *4*, 4845–4851; c) M. N. Popescu, W. E. Uspal, S. Dietrich, *Eur. Phys. J.—Spec. Top.* **2016**, *225*, 2189–2206.

[10] a) L. Huang, J. L. Moran, W. Wang, *JCIS Open* **2021**, *2*, 100006; b) J. Luan, D. Wang, D. A. Wilson, *Nanoscale* **2020**, *12*, 21015–21033; c) H. Wang, M. Pumera, *Chem. Soc. Rev.* **2020**, *49*, 3211–3230.

[11] a) Z. Lin, C. Gao, M. Chen, X. Lin, Q. He, *Curr. Opin. Colloid Interface Sci.* **2018**, *35*, 51–58; b) C. Liu, T. Xu, L.-P. Xu, X. Zhang, *Micromachines* **2018**, *9*, 10; c) J. Bialké, T. Speck, H. Löwen, *J. Non-Cryst. Solids* **2015**, *407*, 367–375.

[12] a) K. Yuan, M. Pacheco, B. Jurado-Sánchez, A. Escarpa, *Adv. Intell. Syst.* **2021**, *3*, 2100002; b) H. Chen, H. Zhang, T. Xu, J. Yu, *ACS Nano* **2021**, *15*, 15625–15644.

[13] a) C. Bechinger, R. Di Leonardo, H. Löwen, C. Reichhardt, G. Volpe, G. Volpe, *Rev. Mod. Phys.* **2016**, *88*, 045006; b) Z. Xiao, M. Wei, W. Wang, *ACS Appl. Mater. Interfaces* **2019**, *11*, 6667–6684; c) J. Katuri, K. Seo, D. Kim, S. Sanchez, *Lab Chip* **2016**, *16*, 1101–1105.

[14] a) A. Brown, W. Poon, *Soft Matter* **2014**, *10*, 4016–4027; b) S. Ebbens, D. Gregory, G. Dunderdale, J. Howse, Y. Ibrahim, T. Liverpool, R. Golestanian, *EPL* **2014**, *106*, 58003; c) J. L. Moran, J. D. Posner, *Phys. Fluids* **2014**, *26*, 042001.

[15] a) A. M. Brooks, M. Tasinkevych, S. Sabrina, D. Velegol, A. Sen, K. J. Bishop, *Nat. Commun.* **2019**, *10*, 495; b) Y. Wang, R. M. Hernandez, D. J. Bartlett, J. M. Bingham, T. R. Kline, A. Sen, T. E. Mallouk, *Langmuir* **2006**, *22*, 10451–10456.

[16] a) A. A. Farniya, M. J. Esplandiu, D. Reguera, A. Bachtold, *Phys. Rev. Lett.* **2013**, *111*, 168301; b) C. Wu, J. Dai, X. Li, L. Gao, J. Wang, J. Liu, J. Zheng, X. Zhan, J. Chen, X. Cheng, *Nat. Nanotechnol.* **2021**, *16*, 288–295.

[17] A. I. Campbell, S. J. Ebbens, P. Illien, R. Golestanian, *Nat. Commun.* **2019**, *10*, 3952.

[18] a) A. T. Brown, W. C. Poon, C. Holm, J. De Graaf, *Soft Matter* **2017**, *13*, 1200–1222; b) X. Zhou, S. Wang, L. Xian, Z. H. Shah, Y. Li, G. Lin, Y. Gao, *Phys. Rev. Lett.* **2021**, *127*, 168001.

[19] a) P. M. Wheat, N. A. Marine, J. L. Moran, J. D. Posner, *Langmuir* **2010**, *26*, 13052–13055; b) J. G. Gibbs, N. A. Fragnito, Y. Zhao, *Appl. Phys. Lett.* **2010**, *97*, 253107.

[20] N. Mano, A. Heller, *J. Am. Chem. Soc.* **2005**, *127*, 11574–11575.

[21] a) R. Liu, A. Sen, *J. Am. Chem. Soc.* **2011**, *133*, 20064–20067; b) W. F. Paxton, K. C. Kistler, C. C. Olmeda, A. Sen, S. K. St Angelo, Y. Cao, T. E. Mallouk, P. E. Lammert, V. H. Crespi, *J. Am. Chem. Soc.* **2004**, *126*, 13424–13431.

[22] J. L. Moran, J. D. Posner, *J. Fluid Mech.* **2011**, *680*, 31–66.

[23] a) W. Wang, W. Duan, A. Sen, T. E. Mallouk, *Proc. Natl. Acad. Sci. USA* **2013**, *110*, 17744–17749; b) I. Theurkauff, C. Cottin-Bizonne, J. Palacci, C. Ybert, L. Bocquet, *Phys. Rev. Lett.* **2012**, *108*, 268303; c) F. Ginot, I. Theurkauff, F. Detcheverry, C. Ybert, C. Cottin-Bizonne, *Nat. Commun.* **2018**, *9*, 696.

[24] a) B. Dai, J. Wang, Z. Xiong, X. Zhan, W. Dai, C.-C. Li, S.-P. Feng, J. Tang, *Nat. Nanotechnol.* **2016**, *11*, 1087–1092; b) T. Maric, M. Z. M. Nasir, R. D. Webster, M. Pumera, *Adv. Funct. Mater.* **2020**, *30*, 1908614; c) R. Dong, Q. Zhang, W. Gao, A. Pei, B. Ren, *ACS Nano* **2016**, *10*, 839–844; d) F. Mou, L. Kong, C. Chen, Z. Chen, L. Xu, J. Guan, *Nanoscale* **2016**, *8*, 4976–4983; e) J. Zhang, J. Song, F. Mou, J. Guan, A. Sen, *Trends Chem.* **2021**, *3*, 387–401.

[25] a) D. Velegol, A. Garg, R. Guha, A. Kar, M. Kumar, *Soft Matter* **2016**, *12*, 4686–4703; b) J. L. Anderson, D. C. Prieve, *Sep. Purif. Methods* **1984**, *13*, 67–103; c) J. Ebel, J. L. Anderson, D. Prieve, *Langmuir* **1988**, *4*, 396–406.

[26] a) D. Prieve, J. Anderson, J. Ebel, M. Lowell, *J. Fluid Mech.* **1984**, *148*, 247–269; b) C. Zhou, H. Zhang, J. Tang, W. Wang, *Langmuir* **2018**, *34*, 3289–3295.

[27] a) M. Ibele, T. E. Mallouk, A. Sen, *Angew. Chem. Int. Ed.* **2009**, *48*, 3308–3312; *Angew. Chem.* **2009**, *121*, 3358–3362; b) X. Wang, L. Baraban, A. Nguyen, J. Ge, V. R. Misko, J. Tempere, F. Nori, P. Formanek, T. Huang, G. Cuniberti, *Small* **2018**, *14*, 1803613.

[28] a) M. Guix, A. K. Meyer, B. Koch, O. G. Schmidt, *Sci. Rep.* **2016**, *6*, 21701; b) J. J. McDermott, A. Kar, M. Daher, S. Klara, G. Wang, A. Sen, D. Velegol, *Langmuir* **2012**, *28*, 15491–15497.

[29] a) H. S. Muddana, S. Sengupta, T. E. Mallouk, A. Sen, P. J. Butler, *J. Am. Chem. Soc.* **2010**, *132*, 2110–2111; b) X. Ma, X. Wang, K. Hahn, S. Sánchez, *ACS Nano* **2016**, *10*, 3597–3605.

[30] N. A. Marine, P. M. Wheat, J. Ault, J. D. Posner, *Phys. Rev. E* **2013**, *87*, 052305.

[31] S. Duan, P. Xu, W. Wang, *Chem. Commun.* **2021**, *57*, 9902–9905.

[32] a) Z. H. Shah, S. Wang, L. Xian, X. Zhou, Y. Chen, G. Lin, Y. Gao, *Chem. Commun.* **2020**, *56*, 15301–15304; b) Y. Gao, R. P. Dullens, D. G. Aarts, *Soft Matter* **2018**, *14*, 7119–7125.

[33] D. Kagan, S. Balasubramanian, J. Wang, *Angew. Chem. Int. Ed.* **2011**, *50*, 503–506; *Angew. Chem.* **2011**, *123*, 523–526.

[34] a) I. Buttinoni, J. Bialké, F. Kümmel, H. Löwen, C. Bechinger, T. Speck, *Phys. Rev. Lett.* **2013**, *110*, 238301; b) Y. Fily, M. C. Marchetti, *Phys. Rev. Lett.* **2012**, *108*, 235702; c) M. E. Cates, J. Tailleur, *Annu. Rev. Condens. Matter Phys.* **2015**, *6*, 219–244.

[35] a) A. Aubret, M. Youssef, S. Sacanna, J. Palacci, *Nat. Phys.* **2018**, *14*, 1114–1118; b) G. S. Redner, M. F. Hagan, A. Baskaran, *Phys. Rev. Lett.* **2013**, *110*, 055701.

[36] a) J. Palacci, S. Sacanna, A. P. Steinberg, D. J. Pine, P. M. Chaikin, *Science* **2013**, *339*, 936–940; b) A. Altemose, M. A. Sánchez-Farrán, W. Duan, S. Schulz, A. Borhan, V. H. Crespi, A. Sen, *Angew. Chem. Int. Ed.* **2017**, *56*, 7817–7821; *Angew. Chem.* **2017**, *129*, 7925–7929; c) W. Gao, A. Pei, R. Dong, J. Wang, *J. Am. Chem. Soc.* **2014**, *136*, 2276–2279; d) M. Chen, Z. Lin, M. Xuan, X. Lin, M. Yang, L. Dai, Q. He, *Angew. Chem.* **2021**, *133*, 16810–16815.

[37] a) B. Liebchen, D. Marenduzzo, M. E. Cates, *Phys. Rev. Lett.* **2017**, *118*, 268001; b) O. Pohl, H. Stark, *Phys. Rev. Lett.* **2014**, *112*, 238303; c) S. Saha, R. Golestanian, S. Ramaswamy, *Phys. Rev. E* **2014**, *89*, 062316.

[38] J. R. Howse, R. A. Jones, A. J. Ryan, T. Gough, R. Vafabakhsh, R. Golestanian, *Phys. Rev. Lett.* **2007**, *99*, 048102.

[39] X. Lyu, X. Liu, C. Zhou, S. Duan, P. Xu, J. Dai, X. Chen, Y. Peng, D. Cui, J. Tang, *J. Am. Chem. Soc.* **2021**, *143*, 12154–12164.

[40] a) S. Eloul, W. C. Poon, O. Farago, D. Frenkel, *Phys. Rev. Lett.* **2020**, *124*, 188001; b) M. De Corato, X. Arqué, T. Patino, M. Arroyo, S. Sánchez, I. Pagonabarraga, *Phys. Rev. Lett.* **2020**, *124*, 108001.

[41] a) D. P. Singh, U. Choudhury, P. Fischer, A. G. Mark, *Adv. Mater.* **2017**, *29*, 1701328; b) D. P. Singh, W. E. Uspal, M. N. Popescu, L. G. Wilson, P. Fischer, *Adv. Funct. Mater.* **2018**, *28*, 1870170; c) T. Yu, P. Chuphal, S. Thakur, S. Y. Reigh, D. P. Singh, P. Fischer, *Chem. Commun.* **2018**, *54*, 11933–11936.

[42] D. P. Singh, W. E. Uspal, M. N. Popescu, L. G. Wilson, P. Fischer, *Adv. Funct. Mater.* **2018**, *28*, 1706660.

[43] B. Jang, W. Wang, S. Wiget, A. J. Petruska, X. Chen, C. Hu, A. Hong, D. Folio, A. Ferreira, S. Pané, *ACS Nano* **2016**, *10*, 9983–9991.

[44] M. J. Esplandiu, K. Zhang, J. Fraxedas, B. Sepulveda, D. Reguera, *Acc. Chem. Res.* **2018**, *51*, 1921–1930.

[45] W. F. Paxton, A. Sen, T. E. Mallouk, *Chem. Eur. J.* **2005**, *11*, 6462–6470.

[46] R. Niu, D. Botin, J. Weber, A. Reinmüller, T. Palberg, *Langmuir* **2017**, *33*, 3450–3457.

[47] a) S. Gáspár, *Nanoscale* **2014**, *6*, 7757–7763; b) H. Yuan, X. Liu, L. Wang, X. Ma, *Bioact. Mater.* **2021**, *6*, 1727–1749; c) S. Ghosh, A. Somasundar, A. Sen, *Annu. Rev. Condens. Matter Phys.* **2021**, *12*, 177–200.

[48] I. A. Pavel, A. I. Bunea, S. David, S. Gáspár, *ChemCatChem* **2014**, *6*, 866–872.

[49] a) K. K. Dey, X. Zhao, B. M. Tansi, W. J. Méndez-Ortiz, U. M. Córdova-Figueroa, R. Golestanian, A. Sen, *Nano Lett.* **2015**, *15*, 8311–8315; b) X. Ma, A. Jannasch, U.-R. Albrecht, K. Hahn, A. Miguel-López, E. Schaffer, S. Sanchez, *Nano Lett.* **2015**, *15*, 7043–7050.

Manuscript received: November 24, 2021
Accepted manuscript online: January 7, 2022
Version of record online: January 27, 2022